PROCEEDINGS, 43rd Workshop on Geothermal Reservoir Engineering
Stanford University, Stanford, California, February 12-14, 2018
SGP-TR-213

Impact of Matrix Permeability on Fracture Transmissivity and Dispersion in Hyperporous Fractured Systems

Bowen Ling[1], Alexandre Tartakovsky[2], Mart Oostrom[2] and Ilenia Battiato[1,*]

1: Green Earth Sciences Building, 367 Panama Street, Stanford, CA 94305

2: Environmental Molecular Science Laboratory, Pacific Northwest National Laboratory, Richland, WA, USA

*ibattiat@stanford.edu

Keywords: Dispersion, Hyperporous, fracture-matrix system

ABSTRACT

Fractured system are ubiquitous to oil, gas and geothermal reservoirs. The transport of mass, heat and momentum within a fractured system is highly dependent on the geometrical properties of the matrix. Current studies of flow and transport in fractures generally assume purely diffusive transport in the matrix. Yet, this assumption is invalid for fractures embedded in hyperporous matrices that can be highly permeable to flow. In this work we provide an overview of the recent models developed for flow and transport in fractured media, as well as their numerical validation. Specifically, we focus on idealized single fracture systems embedded in hyperporous matrices, and on the impact that matrix topology, as characterized by its permeability, has on fracture transmissivity and solute dispersion.

1. INTRODUCTION

Systems with fractures embedded in a porous matrix are common to a variety of engineering processes. Some examples include heat transfer in geothermal reservoirs (Bodvarsson and Tsang 1982, Bommer, et al. 2006, Pruess and Narasimhan 1982) and contaminant transport in fractured rocks, just to mention a few. While the study of heat/mass transport in fractured system has generally focused on fractures embedded in nearly impermeable matrices, many experimental studies have pointed out that dissolution reactions may significantly alter the matrix integrity by inducing cement preferential dissolution, and, as a result, significantly alter the transport properties of the system at a larger scale. One example is represented by calcite cement dissolution during acidic water injection (Noiriel, Made and Gouze 2007, Mangane, Gouze and Luquot 2013). Similarly, in geothermal systems the interaction between unequilibrated waters and fracture minerals can also lead to dissolution and precipitation reactions that may affect long-term reservoir permeability. Among other effects, dissolution processes may lead to cement removal, which ultimately affects the permeability of the matrix in which fractures are embedded (Lammers, Smith and Carroll 2017). Matrix alteration affects heat, mass and momentum transport to the fracture.

From a theoretical standpoint, the difficulty of studying solute/heat transport in coupled fracture-matrix systems lies in the dynamic coupling between the two regions (the fracture and the matrix) and in the need to incorporate different geometrical properties of the matrix into solute transport models at the macroscale. Generally, fractured systems are modelled as two overlapping continua, high permeability fractures and low permeability matrices. These models are generally referred to as dual-porosity models, since the mass/heat exchange between the fracture and the matrix is described by a source term that couples the governing equations for the fracture and to those for the matrix. Upscaling (e.g. by homogenization method, stochastic homogenization, volume averaging) has been one of the techniques routinely used to derive 1D macroscopic models for single fractures. Equations for the average concentration in the fracture $\langle c_f \rangle$ (and the matrix $\langle c_m \rangle$) are derived under the assumption of a thin fracture together with the effective dispersion coefficient in the fracture in terms of effective matrix properties (generally porosity only). Single fracture models are then used as a basis to generalize mass and heat transport equations to fracture systems. Yet, most one-dimensional thin fracture models (Tang, Frind and Sudicky 1981, Dejam, Hassanzadeh and Chen 2014, Bodvarsson and Tsang 1982), as well as two-dimensional dispersion models (Roubinet, Dreuzy and Tartakovsky 2012), assume purely diffusive transport in the matrix (Figure 1, top left), and routinely neglect permeability of and dispersive transport in the matrix (Figure 1, bottom left). Only recently, attempts to account for matrix permeability have been undertaken (Griffiths, Howell and Shipley 2013, Ling, Tartakovsky and Battiato 2016). Ling and *et al*. utilize perturbation theory and upscaling techniques to obtain the fracture dispersion coefficient in terms of matrix porosity and permeability (Ling, Tartakovsky and Battiato 2016). Notwithstanding the variety of proposed models, there is no experimental evidence of their validity. While experiments on real fractured porous media can be conducted, there is little control on porous matrix topology and identification of a relationship between pore-scale matrix structure and fracture dispersion becomes challenging. In this work, we use direct 3D numerical simulations on virtual microfluidic chips to validate two macroscale models developed for transport in a fracture embedded in an impervious (see Figure 1 - left) or a permeable matrix (see Figure 1 - right), respectively.

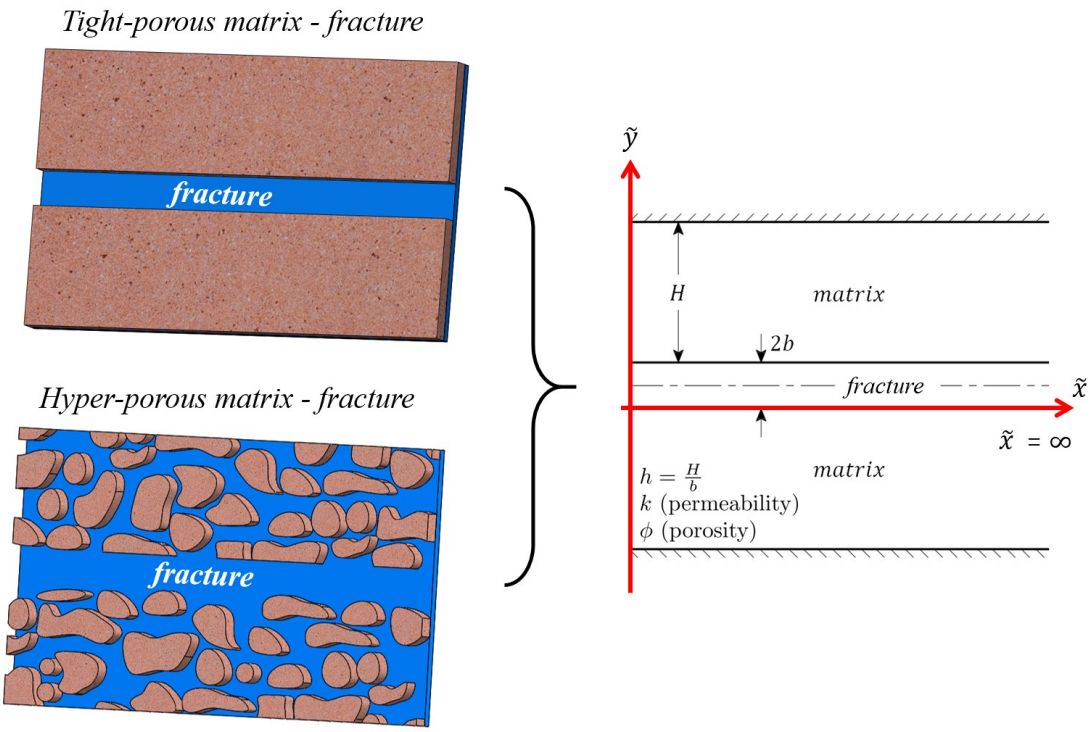

Figure 1: (Left) Fracture coupled with different types of porous matrices. (Right) Effective representation of the domain of interests.

In this paper, we first provide a brief overview of the current macroscale modeling approaches used to analyze passive solute transport in thin porous fractures embedded either in impermeable or permeable matrices. We then use fully resolved pore-scale 3D computational dynamics simulations to investigate the validity of various upscaling approximations. Specifically, we compare 3D pore-scale simulations in synthetically generated micromodels patterned by transverse riblets and arrays of cylinders with two macroscopic transport models developed by Dejam *et al*. (Dejam, Hassanzadeh and Chen 2014) and Ling *et al*. (Ling, Tartakovsky and Battiato 2016) that account for either purely diffusive or dispersive transport in the matrix, respectively. We refer to the model by Dejam, Hassanzadeh, & Chen as 'Diffusive-matrix model' and that by Ling, Tartakovsky, & Battiato as 'Dispersive-matrix model'.

The paper is organized as follows. In section 2, we present three different models (pore-scale model, diffusive-matrix model and dispersive-matrix model), and the impact that matrix permeability has on fracture transmissivity and dispersion. In section 3, we compare fully 3D simulations of transport in synthetically generated micromodels with the two upscaled models. We conclude with a summary of our work in Section 4.

2. NUMERICAL AND ANALYTICAL MODELS: TRASMISSIVITY AND DISPERSION

In this study, we consider transport in three synthetically generated 3D micromodels, M1, M2 and M3 shown in Figure 2. We will compare breakthrough curves calculated from three different upscaled models. The models include: (1) a pore-scale three-dimensional numerical model (denoted as 3D Model); 2) the upscaled diffusive-matrix model developed by Dejam *et al*. (Dejam, Hassanzadeh and Chen 2014); and 3) the upscaled dispersive-matrix model (Ling, Tartakovsky and Battiato 2016).

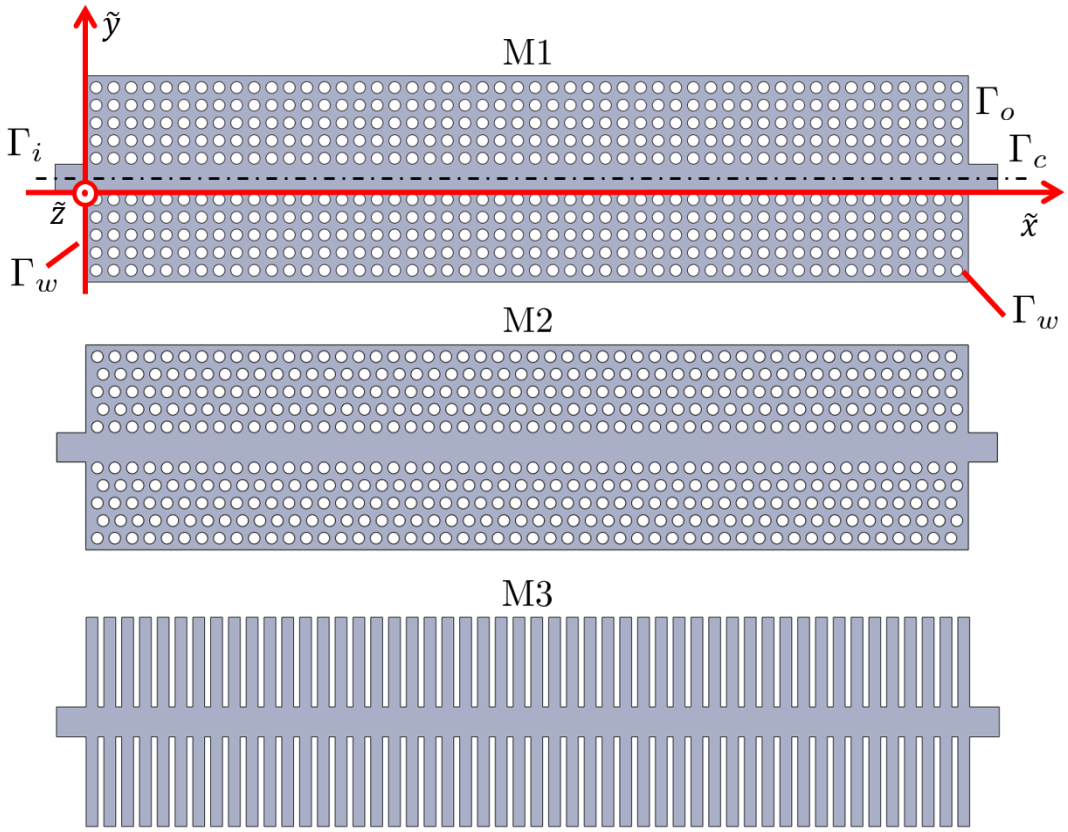

Figure 2: Top view of the synthetically generated 3D micromodels of depth $H_z = 80\ \mu$m and length $L = 15$ mm where a fracture of constant aperture $2b = 0.5$ mm is embedded in three types of matrices, two permeable matrices M1 and M2 constituted of arrays of monodisperse cylinders, and one impervious matrix M3 formed by arrays of riblets transverse to flow.

2.1 Pore-scale model

Flow and passive transport at the pore-scale is governed by the Navier-Stokes, continuity and Advection-Diffusion equations,

$$\frac{\partial \tilde{u}}{\partial \tilde{t}} + (\tilde{u} \cdot \nabla)\tilde{u} + \frac{1}{\rho}\nabla P = \nabla \cdot (\nu \nabla \tilde{u}), \quad (1)$$

$$\nabla \cdot \tilde{u} = 0, \quad (2)$$

$$\frac{\partial c}{\partial \tilde{t}} + \tilde{u} \cdot \nabla c - D_0 \nabla^2 c = 0, \quad (3)$$

where $\tilde{\boldsymbol{u}} = [u, v, w]$ is the velocity vector field, P is the pressure, ρ and ν the density and kinematic viscosity of the fluid, respectively. Since we consider aqueous dilute solutions, the density and viscosity are set to those of water, $\rho = 1000\ \mathrm{kg/m^3}$ and $\nu = 1 \times 10^{-6}\ \mathrm{m^2/s}$.

The physical boundaries of the simulation domain are shown in Figure 2 (top), where we only model half of the entire chip (a symmetry boundary condition is imposed along the channel axis, Γ_c). The inlet and outlet boundaries are denoted as Γ_i and Γ_o, while Γ_w denotes all the impermeable walls, i.e. obstacles, top/bottom surfaces and any other solid surface of the synthetically generated chip. Constant inlet flow rate is imposed on Γ_i, i.e.

$$\tilde{u} = [U, 0, 0], \quad n \cdot \nabla P = 0 \quad \text{for} \quad \tilde{x} \in \Gamma_i, \quad (4)$$

$$n \cdot \nabla \tilde{u} = 0, \quad P = P_{out} \quad \text{for} \quad \tilde{x} \in \Gamma_o, \quad (5)$$

$$\tilde{u} = 0, \quad n \cdot \nabla P = 0 \quad \text{for} \quad \tilde{x} \in \Gamma_w, \quad (6)$$

$$n \cdot \nabla \tilde{u} = 0, \quad n \cdot \nabla P = 0 \quad \text{for} \quad \tilde{x} \in \Gamma_c. \tag{7}$$

2.2 Diffusive-matrix Model

Under the hypothesis that the discrete obstacles can be treated as a porous-continuum impermeable to flow, where mass transport is entirely controlled by diffusion from the channel into the matrix, Dejam *et al*. (Dejam, Hassanzadeh and Chen 2014) upscaled Equations (1) - (3) and derived an equation for the average concentration in the channel and the matrix, $\langle c_f \rangle$ and $\langle c_m \rangle$,

$$\varepsilon Pe \frac{\partial \langle c_f \rangle}{\partial t} + \varepsilon Pe \frac{7}{5} V_m \frac{\partial \langle c_f \rangle}{\partial x} = \varepsilon^2 D_d^* \frac{\partial^2 \langle c_f \rangle}{\partial x^2} - 3\big(\langle c_f \rangle - \langle c_m \rangle\big), \tag{8}$$

$$\varepsilon Pe \frac{\partial \langle c_m \rangle}{\partial t} = D_m \frac{\partial^2 \langle c_m \rangle}{\partial y^2}, \tag{9}$$

where $\varepsilon = b/L$, $Pe = bU/D_0$ is the Peclet number, V_m is the dimensionless average velocity, D_m is the effective molecular diffusion coefficient in the matrix normalized by the molecular diffusion coefficient D_0, $t = \tilde{t}/(L/V)$, $x = \tilde{x}/L$ and $y = \tilde{y}/b$. The dispersion coefficient in the fracture is given by

$$D_d^* = 1 + \frac{1}{175} Pe^2. \tag{10}$$

2.2 Dispersive-matrix Model

Unlike the diffusive-matrix model developed by Dejam *et al*. (Dejam, Hassanzadeh and Chen 2014), Ling et al. by (Ling, Tartakovsky and Battiato 2016) upscaled the pore-scale equations (1) - (3) while explicitly accounting for a permeable matrix with porosity ϕ and permeability k. For low Reynolds numbers, the upscaled flow field satisfies the Stokes equation in the fracture coupled to a Darcy-Brinkman equation in the matrix. For fully developed steady flow conditions, the velocity field admits an analytical solution in the form (Battiato 2012)

$$u_f(y) = -\frac{\Psi}{2}(y^2 + Ay + B), \tag{11}$$

$$u_m(y) = -\frac{\Psi}{\lambda^2}\big(1 + Ee^{\lambda y} + Fe^{-\lambda y}\big), \tag{12}$$

where:

$$\Psi = \frac{b^2}{\mu U} \nabla P, \tag{13}$$

is the dimensionless pressure gradient (with μ the dynamic viscosity and ∇P the dimensional pressure drop) and

$$\lambda = \frac{b}{\sqrt{k}}, \tag{14}$$

is the dimensionless inverse permeability, i.e. the square root of the inverse Darcy number. Another important length scale is the dimensionless height of the matrix, which partly controls the dynamical response of the system at the macroscale (Battiato 2012), defined as

$$\Lambda = \frac{H}{\sqrt{k}}. \tag{15}$$

A matrix is defined 'thick' when $\Lambda > 1$ and 'thin' when $\Lambda < 1$ (Battiato 2012). The integration constants A, B, C and F are defined by

$$A = 2, \tag{16}$$

$$B = 2\lambda^{-2}\big(-1 + e^{\lambda h}\big)\big(-1 + e^{\lambda h} + \lambda + \lambda e^{\lambda h}\big)\big(1 + e^{2\lambda h}\big)^{-1}, \tag{17}$$

$$E = e^{\lambda h}\big(-1 + e^{\lambda h}\big)\big(1 + e^{2\lambda h}\big)^{-1}, \tag{18}$$

$$F = \big(\lambda + e^{\lambda h}\big)\big(1 + e^{2\lambda h}\big)^{-1}. \tag{19}$$

Once the mean velocity profile is analytically determined in terms of λ (i.e. matrix permeability), its impact on trasmissivity can be immediately quantified. Fracture transmissivity is defined as

$$T_f = \frac{Qb}{A\nabla P} \tag{20}$$

where

$$Q = \int_0^b u_f dy, \quad \text{and} \quad A = 2bH_z. \tag{21}$$

In Figure 3, we plot fracture transmissivity in terms of normalized permeability (k/b^2) and different values of the dimensionless height of the matrix h. The Figure demonstrates that the impact of matrix permeability on fracture trasmissivity may be significant, leading to two order-of-magnitude increase for thick and highly permeable matrices. Specifically, the two shades of grey indicate different regimes of Λ (thick or thin matrix). Figure 3 shows that (i) a permeable matrix increases transmissivity of the fracture; (ii) when the matrix is categorized as thick matrix, the influence of the matrix geometry on the transmissivity increases; (iii) when the permeability goes to infinity, the transmissivity reaches a plateau, which corresponds to a fracture with wider aperture.

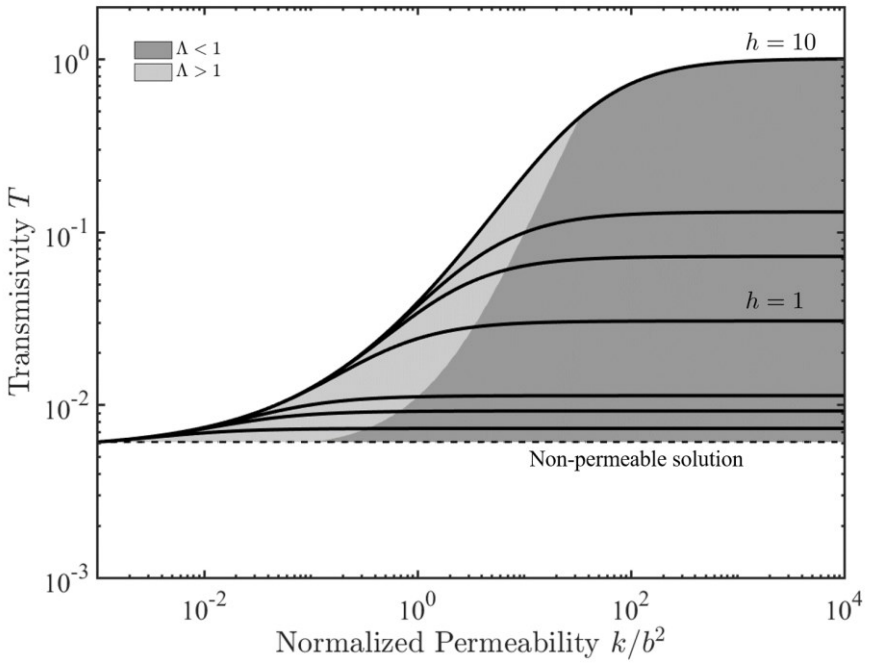

Figure 3: Transmissivity (T) as a function of normalized permeability (k/b^2) for different h and Λ.

Once the mean velocity field is known, homogenization can be further utilized to obtain a macroscopic 1D model for transport. The dispersive-matrix model describes the spatio-temporal evolution of the average pore-scale concentration in the channel and the matrix, $\langle c_f \rangle$ and $\langle c_m \rangle$, up to errors of order ε,

$$Pe\frac{\partial\langle c_f\rangle}{\partial t} + Pe\langle u_f\rangle\frac{\partial\langle c_f\rangle}{\partial x} = \varepsilon D_f^*\frac{\partial^2\langle c_f\rangle}{\partial x^2} + \phi Pe\langle u_m\rangle\frac{\partial\langle c_m\rangle}{\partial x} - \frac{3\phi D_{my}}{\varepsilon^2 h}\big(\langle c_f\rangle - \langle c_m\rangle\big), \tag{22}$$

$$Pe\frac{\partial\langle c_m\rangle}{\partial t} + Pe\langle u_m\rangle\frac{\partial\langle c_m\rangle}{\partial x} = \varepsilon D_m^*\frac{\partial^2\langle c_m\rangle}{\partial x^2} + \frac{Pe}{\phi h}\langle u_f\rangle\frac{\partial\langle c_f\rangle}{\partial x} + \frac{3D_f}{\varepsilon^2\phi h}\big(\langle c_f\rangle - \langle c_m\rangle\big), \tag{23}$$

where D_f is the dimensionless effective molecular diffusion coefficient in the channel and D_{my} is the dimensionless effective molecular diffusion coefficient in the matrix in the y-direction. Here, we set $D_f = D_{my} = 1$, i.e. the effective diffusion coefficients in the fracture and matrix are equal to molecular diffusion.

The velocities $\langle u_f \rangle$ and $\langle u_m \rangle$ in the channel and matrix are the vertically averaged velocity profiles (11) and (12). The dispersion coefficients D_f^* and D_m^*, that explicitly depend on λ (i.e. on the matrix permeability k), are given by

$$D_i^* = 1 + Pe^2 I_i(\lambda, h, \Psi), \tag{24}$$

where

$$I_i = \langle u_i \iint_0^y u_i'(y)\, dydy \rangle, \quad \text{and} \quad u_i'(y) = u_i - \langle u_i \rangle, \quad i = \{f, m\} \tag{25}$$

For the fracture, direct integration gives

$$I_f = \frac{\Psi^2}{105}\left\{1 + \frac{7}{3}\frac{(-1+e^{\lambda h})[-1+e^{\lambda h}+\lambda(1+e^{\lambda h})]}{\lambda^2(1+e^{2\lambda h})}\right\}. \tag{26}$$

Further, to compare newly derived dispersion coefficient with Taylor-Aris dispersion (Taylor 1953) and diffusive model, we define normalized dispersion coefficients as:

$$\kappa_i = \frac{D_i^*}{D_{Taylor-Aris}^*} = \frac{D_i^*}{1+\frac{2}{105}Pe^2}, \quad i = \{f, d\}. \tag{27}$$

In Figure 4, we plot the normalized dispersion coefficient (Taylor 1953). For small Peclet number, $\kappa_f \to \kappa_d$, i.e., the dispersion coefficient for the coupled system with permeable matrix (finite λ) converges to its non-permeable matrix limit independent of h and λ. When $Pe < 1$, advective mixing both in the matrix and channel is negligible relative to diffusive mixing. As a result, $\kappa_f \to \kappa_d$ and $\kappa_d \to 1$. In the intermediate range of Peclet numbers ($1 < Pe < Pe^*$), κ_f changes from $\kappa_f = 1$, to $\kappa_f \to \kappa_f(h, \lambda)$. When $Pe > Pe^*$. It is worth noticing that the dispersion coefficient can overcome its purely diffusive limit when $\lambda < 1$, i.e. mixing is enhanced compared to a channel of half width b. As mentioned above, for large Peclet number, κ_f reaches a Pe-independent asymptotic value $\kappa_f(h, \lambda)$. In this regime, for any given Pe, the dispersion coefficient increases with decreasing λ. This phenomenon is attributed to a decreasing mass flux at the interface between the channel and the matrix, and a resulting decreasing mass loss toward the matrix. Such mass loss is smaller compared with the zero-permeability case, where no solute is transported from the upper steam by the flow in the matrix. This is a newly identified mechanism regulating mass exchange between the channel and the matrix, which is purely controlled by the matrix properties (λ and h) at fixed operating conditions (i.e., constant Pe number). This mechanism is different from the mass transfer mechanism first proposed by Wu and et al. (Wu, Ye and Sudicky 2010) and then quantified by Dejam and et al. (Dejam, Hassanzadeh and Chen 2014) where the channel-matrix interface flux increases (and dimensionless dispersion coefficient κ_d decreases) with increasing Peclet number and is independent of matrix properties λ and h. In the zero permeability limit, i.e., $\lambda \to \infty$, and for fixed Pe, $\kappa_f \to \kappa_d$, as expected.

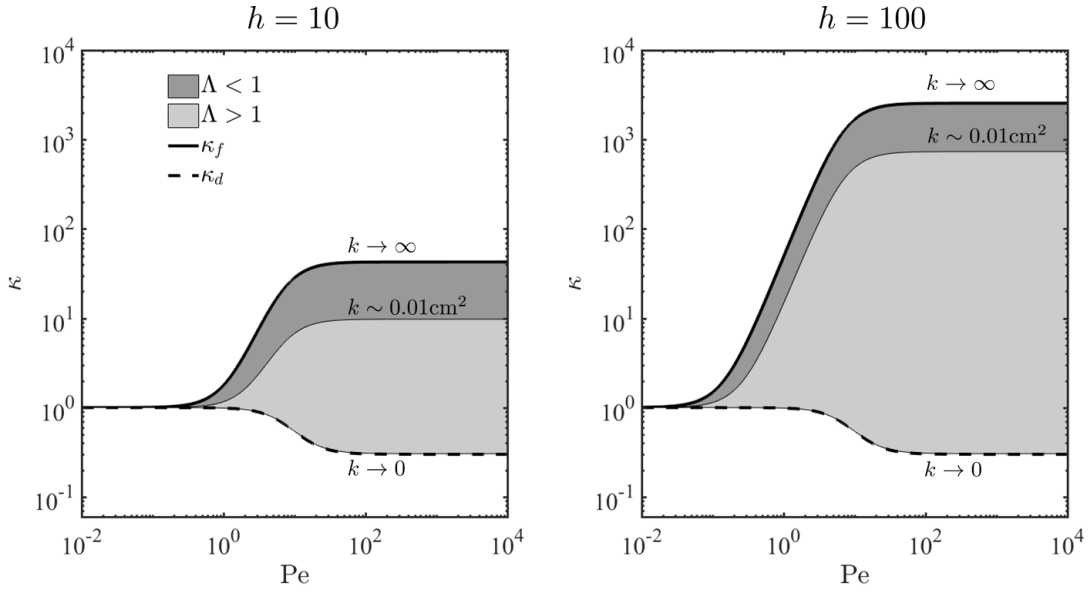

Figure 4: Normalized dispersion coefficients κ_f (solid red lines) and κ_d (dashed back line) versus Pe for different values of λ and Λ . The figure is adapted from Ling and et al.'s work (Ling, Tartakovsky and Battiato 2016).

In the following Section we compare the pore-scale 3D simulations performed on the virtual microchips M1, M2 and M3 as well as the results from the diffusive-matrix and dispersive models.

3. RESULTS AND DISCUSSION

In Figure 5, we plot the breakthrough curves calculated from 3D simulations (solid red lines), and predicted by the diffusive- (dashed black lines) and dispersive-matrix (solid blue lines) models. In the diffusive-matrix model we treat V_m and D_m as a fitting parameters in equation (8) and (9), respectively. In the dispersive-matrix model (equation (22) and (23)) we use Ψ and λ as fitting parameters, instead. The fitting parameters are determined by a least-square algorithm. All fitting results are presented in Figure 5 for different matrix topologies.

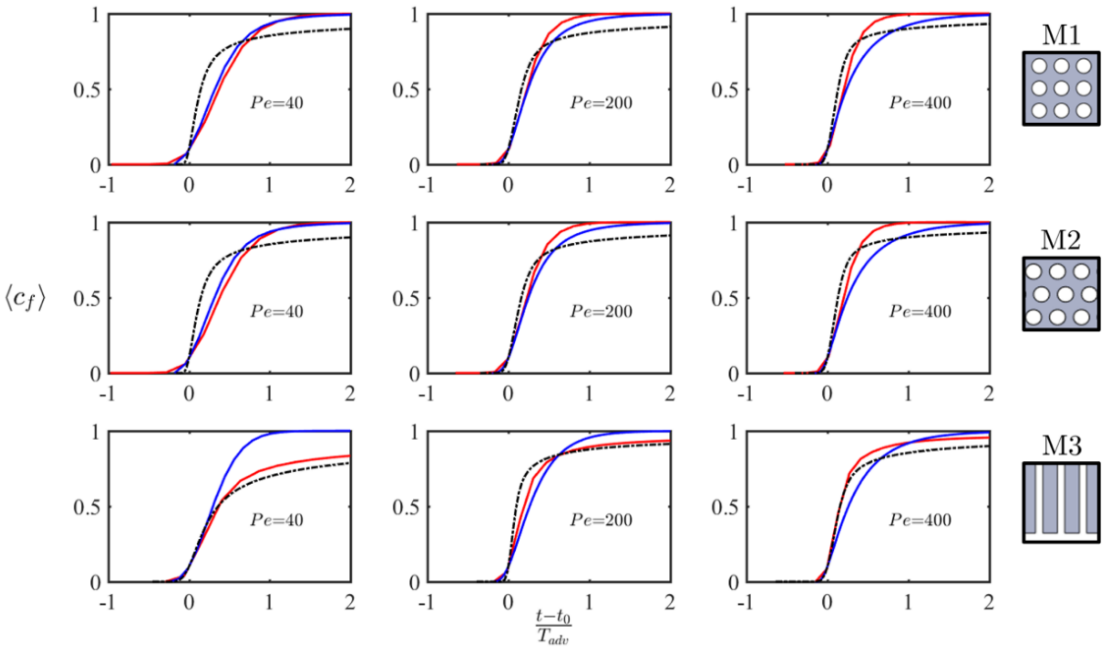

Figure 5: Comparison of breakthrough curves from 3D simulations (solid red lines), diffusive model (black dashed lines) and dispersive model (solid blue lines). The physical time is rescaled and normalized: t_0 represents the time when $c = 0.1$ and $T_{adv} = L/U$.

Figure 5 shows normalized concentration measured at a fixed cross-section along the channel as a function of normalized time. For highly permeable matrix (M1 and M2), the diffusive model (blue solid line) underestimates the breakthrough and presents a long tailing-effect, while the dispersive model captures the pore-scale results and shows a good agreement for different Peclet regimes. On the other hand, the diffusive model captures the breakthrough behavior for impermeable case (M3). This comparison indicates that when the fracture is coupled with a hyper-porous matrix, the breakthrough curve does not exhibit a long tail unlike the diffusive-matrix case. This analysis suggests that matrix permeability has a large impact on macroscopic transport dynamics and that diffusive-matrix models could lead to significant errors predictions, if used to model transport in fractures embedded in hyper-porous media.

4. CONCLUSION

Understanding flow and transport within fractures is essential to a number of natural and industrial processes, including geothermal applications, oil production, etc. Effective models, which are utilized as a substitute of full pore-scale models, generally assume purely diffusive transport in the matrix. However, heterogeneous reactions due to unequilibrated waters may trigger preferential cement dissolution in the matrix embedding the fractures. In this work, we focus on the impact that highly permeable matrices may have on flow and transport in adjacent fractures. We start by reviewing two recently developed upscaled models of passive transport in fractures embedded in impervious and hyperporous matrices. We compare numerical three-dimensional pore-scale simulations of transport in virtual microfluidic chips with the diffusive- and dispersive-matrix models developed by Dejam *et al*. (Dejam, Hassanzadeh and Chen 2014), Ling et al. by (Ling, Tartakovsky and Battiato 2016), respectively. The diffusive-matrix model is routinely applied to predict the breakthrough curves in fracture-matrix. Our simulations conducted on 3D synthetic domains patterned with arrays of cylinders (i.e. hyperporous matrix) and riblets transverse to flow (i.e. impervious matrix) demonstrate that the impact of matrix permeability on macroscale transport cannot be neglected.

Current research includes the design of a set of microfluidic laboratory experiments (i) to validate the 3D numerical code, (ii) to test the model predictivity under different dynamical input and geometries; and (iii) to test the hypothesis that few layer of obstacles can be treated as a porous continuum.

REFERENCE

Auriault, J.-L., and P. M. Adler. "Taylor dispersion in porous media: analysis by multiple scale expansions." *Adv. Water Resour.* 18 (1995): 217-226.

Battiato, I. "Self-similarity in Coupled Brinkman/Navier-Stokes Flows." *J. Fluid Mech.* 699 (2012): 94-114.

Battiato, I., and D. M. Tartakovsky. "Applicability regimes for macroscopic models of reactive transport in porous media." *J. Contam. Hydrol.* 120 (2011): 18-26.

Battiato, I., and J. Vollmer. "Flow-induced shear instabilities of cohesive granulates." *Phys. Rev. E* 86 (2012).

Battiato, I., P. Bandaru, and D. M. Tartakovsky. "Elastic Response of Carbon Nanotube Forests to Aerodynamic Stresses." *Phys. Rev. Lett.* 105 (2010).

Benson, S. M., G. B. Goranson, J. Noble, R. Schroeder, D. Corrigan, and H. Wollenberg. "Evaluation of the Susanville, California geothermal resource Rep." *LBL-11187Lawrence Berkeley Lab., Berkeley, Calif*, 1981.

Bodvarsson, Gudmundur S., and Chin Fu Tsang. "Injection and thermal breakthrough in fractured geothermal reservoirs." *Journal of Geophysical Research: Solid Earth* (Wiley Online Library) 87 (1982): 1031-1048.

Bodvarsson, Gunnar. "Thermal problems in the siting of reinjection wells." *Geothermics* (Elsevier) 1 (1972): 63-66.

Bommer, Julian J., et al. "Control of hazard due to seismicity induced by a hot fractured rock geothermal project." *Engineering Geology* (Elsevier) 83 (2006): 287-306.

Brenner, H. "Dispersion resulting from flow through spatially periodic porous media." *Philos. T. Roy. Soc. A* 297 (1980): 81-133.

Brinkman, H. C. "On the permeability of media consisting of closely packed porous particles." *Appl. Sci. Res.* 1 (1949): 81-86.

Cui, Jiaxi, Daniel Daniel, Alison Grinthal, Kaixiang Lin, and Joanna Aizenberg. "Dynamic polymer systems with self-regulated secretion for the control of surface properties and material healing." *Nat. mater.* (Nature Publishing Group) 14 (2015): 790-795.

Deck, C. P., C. Ni, K. S. Vecchio, and P. R. Bandaru. "The response of carbon nanotube ensembles to fluid flow: Applications to mechanical property measurement and diagnostics." *J. Appl. Physics* 106 (2009): 74304.

Dejam, M., H. Hassanzadeh, and Z. Chen. "Shear dispersion in a fracture with porous walls." *Adv. Water Resour.* 74 (2014): 14-25.

Gilroy, S., and D. L. Jones. "Through form to function: Root hair development and nutrient uptake." *Trends Plant Sci.* 5 (2000): 56-60.

Goharzadeh, Afshin, Arzhang Khalili, and Bo Barker Jorgensen. "Transition layer thickness at a fluid-porous interface." *Phys. Fluids* (AIP Publishing) 17 (2005): 057102.

Griffiths, I. M., P. D. Howell, and R. J. Shipley. "Control and optimization of solute transport in a thin porous tube." *Phys. Fluids* 25 (2013): 033101.

Gruenberger, Alexander, Christopher Probst, Antonia Heyer, Wolfgang Wiechert, Julia Frunzke, and Dietrich Kohlheyer. "Microfluidic Picoliter Bioreactor for Microbial Single-cell Analysis: Fabrication, System Setup, and Operation." *JoVE*, 2013: e50560--e50560.

Horne, R. N., and F. Rodriguez. "Dispersion in tracer flow in fractured geothermal systems." *Geophys. Res. Lett.* 10 (1983): 289-292.

Hou, X., Y. Hu, A. Grinthal, M. Khan, and J. Aizenberg. "Liquid-based gating mechanism with tunable multiphase selectivity and antifouling behaviour." *Nature* 519 (2015): 70-73.

Lammers, Kristin, Megan M Smith, and Susan A Carroll. "Muscovite dissolution kinetics as a function of pH at elevated temperature." *Chemical Geology*, 2017: 149--158.

Ling, Bowen, Alexandre M. Tartakovsky, and Ilenia Battiato. "Dispersion controlled by permeable surfaces: surface properties and scaling." *J. Fluid Mech.* (Cambridge Univ Press) 801 (2016): 13-42.

Ling, Bowen, Mart Oostrom, Alexandre Tartakovsky, and Ilenia Battiato. "Hydrodynamic dispersion in thin porous channels with controlled microtexture." *Submitted to Physics of Fluids*, 2018: .

Liu, Chongxuan, Jianying Shang, Sebastien Kerisit, John M. Zachara, and Weihuang Zhu. "Scale-dependent rates of uranyl surface complexation reaction in sediments." *Geochim. Cosmochim. Ac.* (Elsevier) 105 (2013): 326-341.

Mangane, Papa O, Philippe Gouze, and Linda Luquot. "Permeability impairment of a limestone reservoir triggered by heterogeneous dissolution and particles migration during CO2-rich injection." *Geophysical Research Letters*, 2013: 4614--4619.

Marschner, Horst, and B. Dell. "Nutrient uptake in mycorrhizal symbiosis." *Plant Soil* (Springer) 159 (1994): 89-102.

Nikora, Vladimir, Derek Goring, Ian McEwan, and George Griffiths. "Spatially averaged open-channel flow over rough bed." *J. Hydraul. Eng.* (American Society of Civil Engineers), 2001.

Nitsche, L. C., and H. Brenner. "Eulerian kinematics of flow through spatially periodic models of porous media. ." *Arch. Ration. Mech. Anal.* 107 (1989): 225-292.

Noiriel, Catherine, Benoit Made, and Philippe Gouze. "Impact of coating development on the hydraulic and transport properties in argillaceous limestone fracture." *Water resources research*, 2007.

Petravek, Zdenek, and Petra Schwille. "Precise measurement of diffusion coefficients using scanning fluorescence correlation spectroscopy." *Biophys. J.* (Elsevier) 94 (2008): 1437-1448.

Pruess, K., and T. N. Narasimhan. "On fluid reserves and the production of superheated steam from fractured, vapor-dominated geothermal reservoirs." *Journal of Geophysical Research: Solid Earth* (Wiley Online Library) 87 (1982): 9329-9339.

Roubinet, D., J.-R. Dreuzy, and D. M. Tartakovsky. "Semi-analytical solutions for solute transport and exchange in fractured porous media." *Water Resour. Res.* 48 (2012).

Stroock, A. D., S. K. W. Dertinger, A. Ajdari, I. Mezic, H. A. Stone, and G. M. Whitesides. "Chaotic mixer for microchannels." *Science* 295 (2002): 647-651.

Tang, D. H., E. O. Frind, and E. A. Sudicky. "Contaminant transport in fractured porous media: Analytical solution for a single fracture." *Water Resour. Res.* 17 (1981): 555-564.

Taylor, G. "Dispersion of soluble matter in solvent flowing slowly through a tube." *P. R. Soc. London.* 1953. 186-203.

Whitaker, S. *The Method of Volume Averaging.* Netherlands: Kluwer Academic Publishers, 1999.

Willingham, Thomas, Changyong Zhang, Charles J. Werth, Albert J. Valocchi, Mart Oostrom, and Thomas W. Wietsma. "Using dispersivity values to quantify the effects of pore-scale flow focusing on enhanced reaction along a transverse mixing zone." *Adv. Water Resour.* (Elsevier) 33 (2010): 525-535.

Wu, Y.-S., M. Ye, and E. A. Sudicky. "Fracture-flow-enhanced matrix diffusion in solute transport trhough fractured porous media." *Transp. Porous Med.* 81 (2010): 21-34.

Zhang, Changyong, et al. "Pore-scale study of transverse mixing induced CaCO3 precipitation and permeability reduction in a model subsurface sedimentary system." *Environ. Sci. Technol.* (ACS Publications) 44 (2010): 7833-7838.